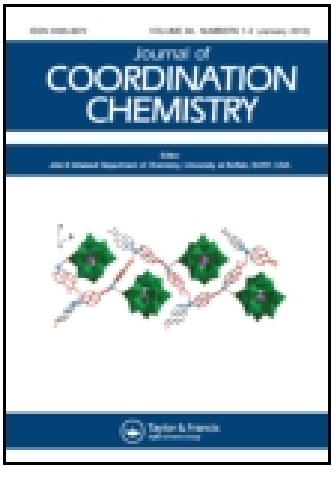

Journal of Coordination Chemistry
Publication details, including instructions for authors and subscription information:
http://www.tandfonline.com/loi/gcoo20

Polyoxometalate cobalt-gatifloxacin complex with DNA binding and antibacterial activity

Hong Liu[a], Yu-Long Zou[a], Lei Zhang[a], Jian-Xun Liu[a], Chao-Yu Song[a], Dong-Feng Chai[a], Guang-Gang Gao[ab] & Yun-Feng Qiu[c]

[a] College of Pharmacy, Jiamusi University, Jiamusi, China

[b] Department of Chemistry, Changchun Normal University, Changchun, China

[c] State Key Lab of Urban Water Resource and Environment (SKLUWRE) & Academy of Fundamental and Interdisciplinary Science, Harbin Institute of Technology, Harbin, China

Accepted author version posted online: 04 Jul 2014.Published online: 25 Jul 2014.

To cite this article: Hong Liu, Yu-Long Zou, Lei Zhang, Jian-Xun Liu, Chao-Yu Song, Dong-Feng Chai, Guang-Gang Gao & Yun-Feng Qiu (2014) Polyoxometalate cobalt-gatifloxacin complex with DNA binding and antibacterial activity, Journal of Coordination Chemistry, 67:13, 2257-2270, DOI: 10.1080/00958972.2014.940923

To link to this article: http://dx.doi.org/10.1080/00958972.2014.940923

Journal of Coordination Chemistry, 2014
Vol. 67, No. 13, 2257–2270, http://dx.doi.org/10.1080/00958972.2014.940923

Polyoxometalate cobalt–gatifloxacin complex with DNA binding and antibacterial activity

HONG LIU†, YU-LONG ZOU†, LEI ZHANG†, JIAN-XUN LIU†, CHAO-YU SONG†, DONG-FENG CHAI†, GUANG-GANG GAO*†‡ and YUN-FENG QIU*§

†College of Pharmacy, Jiamusi University, Jiamusi, China
‡Department of Chemistry, Changchun Normal University, Changchun, China
§State Key Lab of Urban Water Resource and Environment (SKLUWRE) & Academy of Fundamental and Interdisciplinary Science, Harbin Institute of Technology, Harbin, China

(*Received 17 March 2014; accepted 6 June 2014*)

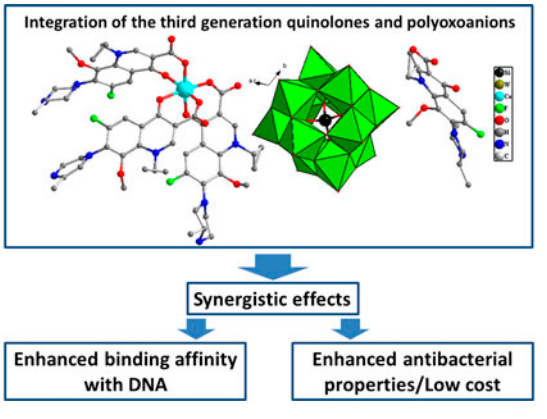

An unusual inorganic–organic antibacterial complex based on polyoxometalates (POMs) and the cobalt–gatifloxacin (GT), $[Co^{II}(C_{19}FH_{22}N_3O_4)_3][C_{19}FH_{23}N_3O_4][HSiW_{12}O_{40}]\cdot 23H_2O$ (**1**), has been synthesized. Single-crystal structural analysis shows that **1** represents for the first time an unusual tripodal coordination style with three GT molecules coordinating to cobalt(II) by six carboxylate and hydroxyl oxygens. The biological activity of **1** has been evaluated by investigating its binding ability to calf thymus DNA (CT-DNA). UV spectrum study of **1** has shown that it can bind to CT-DNA by intercalation. The DNA-binding constant K_b was $9.6 \times 10^4\,M\,L^{-1}$, higher than that of pure GT, $3.8 \times 10^4\,M\,L^{-1}$. Furthermore, the antibacterial activities of **1** were tested against *Staphylococcus aureus* and *Escherichia coli*, respectively, and have shown slightly lower antibacterial activity than that of free GT at the same mass concentration. If the GT component in the complexes was controlled at the same molar concentration, **1** generates the biggest antibacterial area during the Kirby–Bauer disc diffusion detection. This result indicates that the integration of heteropolyanions and GT exhibits synergistic effects on the antibacterial activity, which paves a new way to design low-cost antibacterial compound by the introduction of POMs.

Keywords: Polyoxometalate; Gatifloxacin; Fluorescence quenching; DNA binding; Antibacterial

*Corresponding authors. Email: gaogg@jmsu.edu.cn (Guang-Gang Gao); qiuyf@hit.edu.cn (Yun-Feng Qiu)

1. Introduction

Quinolones are an important family of highly potent broad-spectrum antibacterial agents widely used in clinical practice for the treatment of various infections. The targets of quinolones are both gyrases and topoisomerases and further lead to inhibition of DNA replication [1]. Overdosing on quinolones has led to increasing resistance to antibiotics, which is common among *Pseudomonas aeruginosa* and *Staphylococcus* spp. and some initially more susceptible pathogens, such as *Escherichia coli* and *Salmonella* spp. [2–4]. In order to decrease the resistance of bacteria to antibiotics, more metal–quinolone complexes have been synthesized and some of them are reported to possess improved water solubility and antibacterial activity [5].

Gatifloxacin (GT),(±)-1-cyclopropyl-1,4-dihydro-6-fluoro-8-methoxy-7-(3-methyl-1-piperazinyl)-4-oxo-3-quinolinecarboxylic acid, belongs to third-generation quinolones and is an effective antibacterial agent. To date, it has been used for the treatment of infections of the lungs and skin mainly due to its wide spectrum of activity [6]. Inspired by previous reports, the introduction of metal ion into the hybrid structure of antibiotics enhances the antibacterial activities due to the synergistic effects of individual components. So far, only a few single-crystal structural GT-based complexes are reported. In 2007, $M(GT)_2(H_2O)_2{\cdot}4H_2O$ (M = Zn, Ni, Co) was synthesized [7], in which different metal ions in the structures cause GT to exhibit varied activities against *Staphylococcus*. The Zn(II) and the Ni(II) complexes result in enhancement of antibacterial activities against *Staphylococcus*, whereas the Co(II) complex showed decreased activity. Patel and co-workers studied the synthesis of single-crystal of Cu(II) and Pt(II) complexes of GT and their abilities to bind to HS-DNA [8]. Crystal structures of cobalt complexes of pipemidic acid [9], enrofloxacin [10], and norfloxacin [11] have also been reported.

Polyoxometalates (POMs), as antitumor, antibacterial and antiviral inorganic medical agents, are attractive inorganic compounds for applications in medicine [12, 13]. Supramolecular complexes based on POMs have been investigated, in which POMs functioned as inorganic linkers or counter anions. The as-prepared hybrid materials have been applied in many important aspects of chemistry, such as catalysis, non-linear optical, biosensor, and chemotherapy agents [14–16]. POMs often act as additives or rigid templates to help control the outcome of a reaction and have been introduced into hybrid materials [17]. Up to date, POMs as templates introduced into organic or inorganic components have been widely studied, as a result of enriching their structures and improving properties of the hybrids because of the intrinsic properties of individual components and the integration of their merits [18]. Recently, some transition-metal–quinolone complexes modified by POMs have been reported. Among these complexes, quinolones mainly include first and second generations, such as pipemidic acid, enrofloxacin and norfloxacin [19–21], while POM-based transition-metal–GT complex, that is the third-generation complex, remains unreported. Additionally, considering the superior properties of POMs, it is speculated that the introduction of them in the synthesis may not only induce the formation of compounds, but also afford synergistic antibacterial properties, and thus lower the cost of antibiotics as POMs are inexpensive comparing with the organic quinolones.

Here, Keggin-type polyoxoanion, $[SiW_{12}O_{40}]^{4-}$ (SiW_{12}), was selected as a template agent due to its facile synthesis and stability against surrounding environments. An inorganic–organic antibacterial complex, $[Co^{II}(C_{19}FH_{22}N_3O_4)_3][C_{19}FH_{23}N_3O_4][HSiW_{12}O_{40}]{\cdot}23H_2O$ (**1**), has been synthesized by conventional solution approach. Energy transfer between GT and POMs was evaluated in terms of fluorescence quenching. The binding affinity of **1** with

calf thymus DNA (CT-DNA) was also studied. The antibacterial activities of **1** have also been investigated.

2. Experimental

2.1. *Materials and methods*

All chemicals of reagent grade were purchased from commercial sources and used without purification. Elemental analyses (C, H, and N) were performed on a Perkin Elmer 240 CHN elemental analyzer. IR spectra were obtained on an Alpha Centauri FT/IR spectrometer with KBr pellet from 400 to 4000 cm^{-1}. UV–visible spectra were recorded in a UV-2550. Fluorescence spectra were measured in solution on a 970CRT spectrofluorescence instrument. $K_8[SiW_{11}O_{39}]\cdot 13H_2O$ and $Co(GT)_2(H_2O)_2\cdot 4H_2O$ (denoted as $Co(GT)_2$) were prepared according to literature methods [7, 22]. DNA stock solution was prepared by dilution of CT-DNA to buffer solution (50 mL of 0.1 M/L tris solution and 42 mL of 0.1 M/L hydrochloric acid, diluted to 100 mL) followed by vigorous stirring at 4 °C for 3 days, and kept at 4 °C for not longer than a week. The ratio of UV absorbance values at 260 and 280 nm (A260/A280) of CT-DNA stock solution is 1.89, indicating that the DNA was sufficiently free of protein contamination [23]. The DNA concentration was determined by the UV absorbance at 260 nm after 1 : 20 dilution using $\varepsilon = 6600$ M/L cm^{-1} [24].

2.1.1. General procedure for the synthesis of $[Co(C_{19}FH_{22}N_3O_4)_3]$-$[C_{19}FH_{23}N_3O_4][HSiW_{12}O_{40}]\cdot 23H_2O$ (1). $K_8[SiW_{11}O_{39}]\cdot 13H_2O$ (0.97 g, 0.3 mM) and $CoCl_2\cdot 6H_2O$ (0.048 g, 0.2 mM) were dissolved in 20 mL water. Then, 20 mL water solution of GT (0.15 g, 0.4 mM) and $CoCl_2\cdot 6H_2O$ (0.048 g, 0.2 mM) was added to the above solution. The pH of the mixture was adjusted to 3.8 using 0.1 M L^{-1} NaOH under stirring, and then the solution was heated at 95 °C for 3.0 h. The filtrate was kept for one month at ambient conditions, then red block crystals of **1** (30% yield based on Co) were filtered, washed with water, and dried at room temperature. Elemental analyses Calcd for $C_{76}CoF_4H_{136}N_{12}O_{79}SiW_{12}$ (4851.02): C, 18.82; N, 3.46; H, 2.83. Found: C, 18.70; N, 3.42; H, 2.75. IR (KBr, cm^{-1}): 3429(s), 2974(w), 2927(w), 2854(w), 1728(w), 1617(m), 1565(w), 1525(w), 1447(m), 1401(w), 1368(w), 1322(w), 1221(w), 1171(w), 1093(w), 1053(w), 955(w), 949(w), 897(m), 789(m), 701(w), 530(w).

2.1.2. X-ray crystal structure determination. Crystal data for **1** were collected on a Bruker Smart Apex-II CCD diffractometer with Mo Kα monochromatic radiation ($\lambda = 0.71073$ Å) at room temperature. The structure was solved by direct methods and refined by full matrix least-squares on F^2 using SHELXTL crystallographic software package [25, 26]. All metal ions were refined anisotropically. Parts of disordered oxygen and carbon were refined isotropically and some occupancies were set as 50% to accomplish good refinement. The positions of hydrogens on carbon were calculated theoretically. The crystal data and structure refinement of **1** are summarized in table 1.

2.1.3. Antimicrobial tests. The antibacterial activity of **1** was studied against *Staphylococcus aureus* and *E. coli* by determining the minimum inhibitory concentration (MIC) and a modified Kirby–Bauer disc diffusion method.

Table 1. Crystal data and structure refinement for **1**.

Empirical formula	$C_{145}H_{167}Co_2F_8N_{24}O_{140}Si_2W_{24}$	
Formula weight	9224.47	
Wavelength	0.71073 Å	
Crystal system	Triclinic	
Space group	*P–I*	
Unit cell dimensions	$a = 17.8188(3)$ Å	$\alpha = 108.4880(10)°$
	$b = 19.9982(4)$ Å	$\beta = 97.6140(10)°$
	$c = 20.9012(4)$ Å	$\gamma = 107.3310(10)°$
Volume	6527.6(2) $Å^3$	
Z	1	
Absorption coefficient	10.758 mm^{-1}	
$F(0\,0\,0)$	4255	
θ range for data collection	1.84°–27.5°	
Reflections collected/unique	100,313/29,822 [$R_{int} = 0.1135$]	
Completeness to θ	99.6%	
Refinement method	Full-matrix least-squares on F^2	
Data/restraints/parameters	29,822/7/1381	
Goodness-of-fit on F^2	1.001	
Final R indices [$I > 2\sigma(I)$]	$R_1 = 0.0729$, $wR_2 = 0.1864$	
R indices (all data)	$R_1 = 0.1821$, $wR_2 = 0.2387$	
Largest diff. peak and hole	1.98 and –5.163 e A^{-3}	

2.1.3.1. *Kirby–Bauer disc diffusion method. S. aureus* and *E. coli* were freshly isolated from clinical material and dissolved in 15 mL of sterilized agar culture media at 40 °C and inoculated on a sterilized culture dish. The bacterial suspensions were incubated at 37 °C for 24 h. Then, nutrient agar was sterilized at 121 °C for about 20 min and poured into the Petri dishes with a thickness of 3 mm. Then, 0.1 mL diluted bacterial suspension of *E. coli* was spread uniformly on the surface of the nutrient agar. Thirty minutes later, the as-prepared filter paper slices were placed on the bacteria. The Petri dishes were incubated at 37 °C for 12 h. The diameters of the inhibition zones were measured by caliper and the results were recorded by camera.

2.1.3.2. *Minimum inhibitory concentration.* The MIC was defined as the lowest concentration of antimicrobial agent showing complete inhibition of growth. MIC was determined using twofold serial dilutions in liquid media containing 160–0.02 μg mL^{-1} of the compound being tested. Free GT was tested as a reference compound.

2.1.4. DNA binding studies. The interaction of complexes with CT-DNA has been studied with UV spectroscopy to investigate the possible binding mode to CT-DNA and to calculate the binding constants to CT-DNA (K_b). In UV titration experiments, the spectra of CT-DNA in the presence of complexes have been recorded for a constant CT-DNA concentration at diverse [complex]/[CT-DNA] mixing ratios. The intrinsic binding constants K_b of the complexes with CT-DNA have been determined using UV spectra recorded for a constant concentration in the absence or presence of CT-DNA.

3. Results and discussion

3.1. *Synthesis*

Generally, transition metal ions coordinate to quinolone ligands through carbonyl and carboxyl groups to form ML_2 complexes. Most of these complexes have planar configuration for the transition metal cations. Very few complexes are ML_3 or ML types, such as $[Co(HEx)_2(Ex)]Cl{\cdot}2CH_3OH{\cdot}12H_2O$ (Ex = Enoxacin) and $Co(Cx)Na{\cdot}6H_2O$ (Cx = Cinoxacin) [27, 28]. To obtain new inorganic–organic compounds, we selected POMs as synthetic modulators due to their robust structure, potential antibacterial performance, simple synthesis, as well as being low-cost inorganic additives for medicines. Under hydrothermal conditions, introduction of Keggin-type SiW_{12} into the reaction system successfully leads to isolation of single crystalline materials of **1**. We have also tried to synthesize **1** without SiW_{12}, unfortunately, only unidentified powder can be found in the final product. Therefore, the introduced SiW_{12} polyoxoanion plays a key role in the formation of **1**. This may relate to the fact that POM anions are usually surface oxygen abundant clusters, which may induce the coordination activity of organic ligands due to weak interactions, such as hydrogen bonding or van der Waals forces.

3.2. *Crystal structure*

Single-crystal X-ray structural analysis reveals that **1** is constructed from SiW_{12} polyoxoanion, $[Co^{II}(GT)_3]$, isolated GT, and isolated water molecules, as shown in figure 1. The introduced SiW_{12} is a classical α-Keggin type polyoxoanion, which contains four W_3O_{13} units and one ordered $[SiO_4]^{4-}$ in the center with Si–O bonds ranging from 1.556(13) to 1.668(12) Å. The W–O bond distances are divided into three groups: 1.691(12)–1.862(16) Å for $W–O_t$; 1.882(13)–1.995(14) Å for $W–O_{b/c}$; and 2.237(13)–2.381(12) Å for $W–O_a$

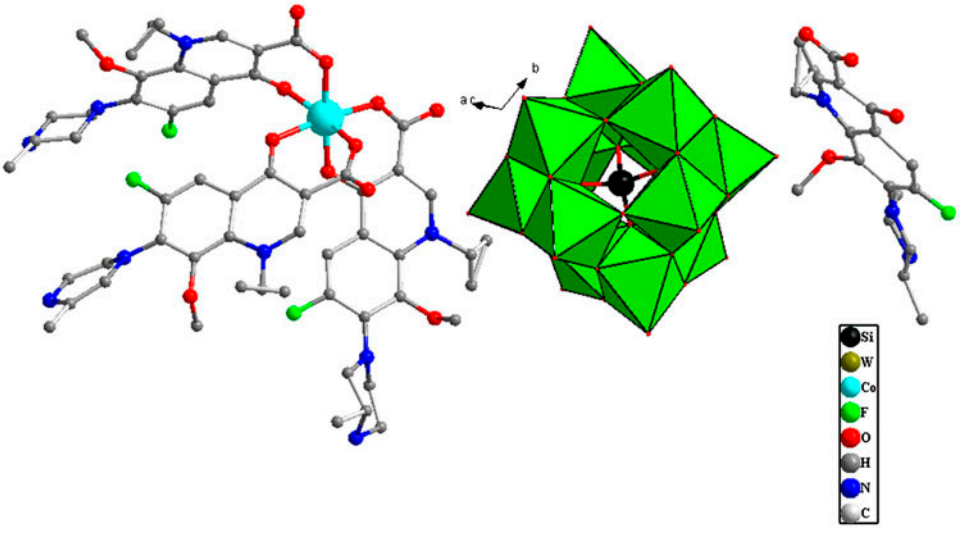

Figure 1. Combined polyhedra and ball–stick view of **1** (water molecules and all hydrogen atoms are omitted for clarity).

(O_t, terminal oxygen atoms; $O_{b/c}$, μ_2- or μ_3-bridging oxygen atoms; O_a, central oxygen atoms linking Si). The valence sum calculations [29] show that all the W ions are in the +6 oxidation states and Co ions are +2. Co^{2+} in $[Co(GT)_3]$ is six-coordinate by six oxygens from carboxylate or hydroxyl groups arising from three GT ligands, showing an octahedral coordination environment. To the best of our knowledge, it is the first time that tripodal coordination pattern has been observed in transition-metal quinolone complexes. The $Co–O_{hydroxyl}$ bond lengths are slightly longer than those of $Co–O_{carboxylic}$, in which the $Co–O_{hydroxyl}$ distances are 2.046(13)–2.105(11) Å, while the $Co–O_{carboxylic}$ distances range from 2.032(14) to 2.088(16) Å. Selected coordination parameters can be found in table 2. Though **1** contains polyoxoanion and water, it remains almost insoluble in water. Structural analysis of **1** indicates that $[Co(GT)_3]$ and isolated GT are located around each polyoxoanion. The $\pi\cdots\pi$ stacking interactions can be found between each pair of $[Co(GT)_3]$ units or isolated GT molecules, of which the centroid–centroid distances are 3.754 Å or 4.012 Å, respectively (as shown in figure 2). There also exists N–H···O hydrogen bonding interactions between piperazinyl N and terminal O from polyoxoanions. Short distances between terminal O of polyoxoanion and aromatic rings belonging to GT are observed, and for the first time weak interactions between polyoxoanion oxygen and aromatic ring have been observed. The distances of O···Centroid are 2.890 and 3.312 Å, respectively. In addition, possible hydrogen bonding interactions also exists between O from free water and N or O from GT or polyoxoanions. All the above weak interactions consolidate the stability of **1** and result in its insolubility in water.

3.3. *FT-IR spectra studies*

As seen in figure 3, FT-IR of SiW_{12} has four characteristic bands at 1020, 980, 926, and 782 cm^{-1} ascribed to $Si–O_a$ asymmetrical, $W{=}O_d$ asymmetrical, $W–O_b–W$ asymmetrical, and $W–O_c–W$ asymmetrical vibrations, respectively [30]. O_a, O_b, O_c, and O_d are referred to oxygens connected to silicon, to oxygens bridging to two tungstens (from two different W_3O_{13} for O_b and from the same W_3O_{13} for O_c), and to the terminal oxygen W=O, respectively. FT-IR spectrum of **1** exhibits four asymmetric vibrations at 998, 955, 897, and 789 cm^{-1}, which

Table 2. Selected bond lengths (Å) and angles (°) for **1**.

Bond	Distance	Bond	Angle
Si–O (40)	1.556(13)	O(40)–Si–O(38)	111.1(6)
Si–O(38)	1.613(11)	O(40)–Si–O(37)	109.6(6)
Si–O(37)	1.631(11)	O(38)–Si–O(37)	108.6(6)
Si–O(39)	1.668(12)	O(40)–Si–O(39)	110.6(6)
Co–O(49)	2.032(14)	O(38)–Si–O(39)	109.9(6)
Co–O(51)	2.046(13)	O(37)–Si–O(39)	107.0(7)
Co–O(45)	2.080(12)	O(49)–Co–O(51)	86.7(6)
Co–O(47)	2.083(13)	O(49)–Co–O(45)	92.8(6)
Co–O(41)	2.088(16)	O(51)–Co–O(45)	88.7(6)
Co–O(43)	2.105(11)	O(49)–Co–O(47)	173.2(6)
W(1)–O(1)	1.862(16)	O(51)–Co–O(47)	86.6(5)
W(1)–O(4)	1.882(13)	O(45)–Co–O(47)	85.7(5)
W(1)–O(5)	1.889(13)	O(49)–Co–O(41)	90.3(6)
W(1)–O(8)	1.981(14)	O(51)–Co–O(41)	176.9(5)
W(1)–O(7)	1.995(14)	O(45)–Co–O(41)	90.4(6)
W(1)–O(39)	2.237(13)	O(47)–Co–O(41)	96.3(6)

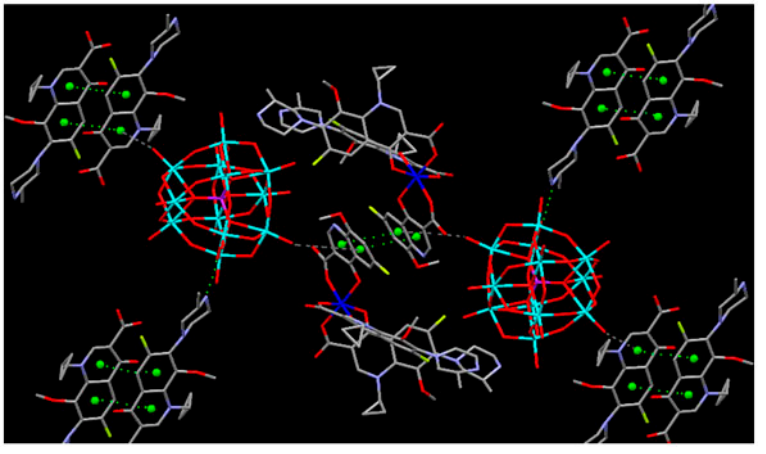

Figure 2. Ball–stick view of **1** with weak interactions (all water molecules and parts of cyclopropyl and piperazinyl groups in $Co(GT)_3$ units were omitted for clarity).

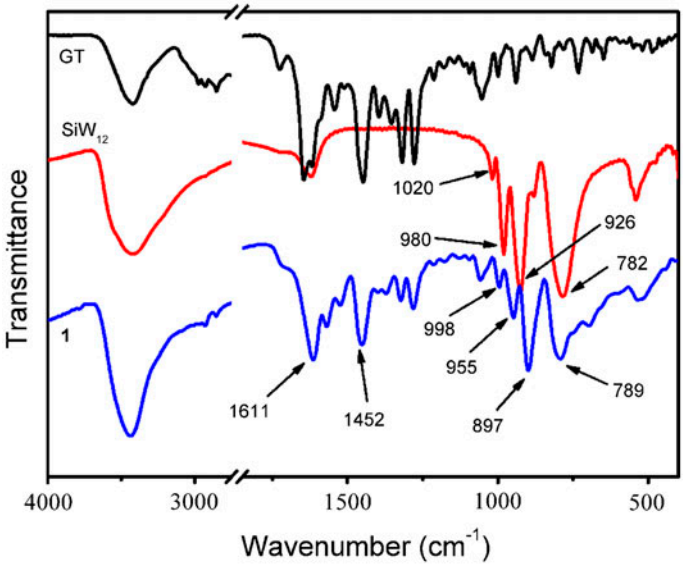

Figure 3. FT-IR spetra of GT, SiW_{12}, and **1**. The arrows indicate the characteristic peaks of Si–O_a, W–O_t, and W–$O_{b/c}$ in SiW_{12} and **1**. FT-IR was measured by KBr pellets.

are similar to those bands in SiW_{12} polyoxoanion. The characteristic peaks confirmed that the SiW_{12} Keggin structures are intact in **1**. Slight change of these asymmetric vibrations indicates strong interactions between polyoxoanions and organic ligands, consistent with the single-crystal structure. Bands centered at 1611 and 1452 cm^{-1} can be assigned as (O–C–O) asymmetric and symmetric stretching vibrations in the spectrum of **1**. The strong vibration at 3429 cm^{-1} indicates the existence of water molecules distributed in the crystal structure.

3.4. *Fluorescence quenching studies*

The strong interactions between SiW_{12} and GT have also been evaluated by titration experiments. Polyoxoanions could serve as electron reservoirs to transfer the photo-induced carriers from semiconductor surface, and thus retard the recombination of electrons and holes [31, 32]. Meanwhile, the fluorescent quenching phenomena of semiconductors or organic compounds always occurred when contacting with polyoxoanions via covalent or non-covalent bonds, which is a solid proof for the existence of energy transfer or electron transfer between donor and acceptor [33, 34]. In order to check the interactions between SiW_{12} and GT, GT aqueous solution was titrated by varied concentration of SiW_{12} solution. Figure 4 illustrates the fluorescence spectra of GT as a function of increasing amounts of SiW_{12}. It is obvious to see that the fluorescent intensity at 480 nm corresponding to GT emission decreased gradually as the SiW_{12} concentration increased. When the molar ratio of GT and SiW_{12} reach 1 : 0.36, 94% fluorescent intensity was quenched. The efficient quenching could be ascribed to energy transfer or electron transfer between GT and SiW_{12}, in which the strong interactions might be hydrogen bonding or electrostatic interactions. The distances of O···Centroid are 2.890 and 3.312 Å in crystals, which are much closer than those in aqueous solution (van der Waals distances in the presence of solvent molecules), thus it is assumed that the fluorescent quenching efficiency will be much higher than that in solution [35, 36]. Therefore, we speculate that the strong interactions between polyoxoanions and ligands will result in interesting antibacterial properties due to the positive synergistic effects.

3.5. *Antibacterial studies*

Quinolones and its derivatives are clinical antibacterial agents for the treatment of infections. In some cases, the metal complexes of drugs are more active than their parent compounds [37, 38]. Based on these results, metal compounds of quinolones have been synthesized to evaluate their antibacterial activity [39, 40]. In this paper, the studies were

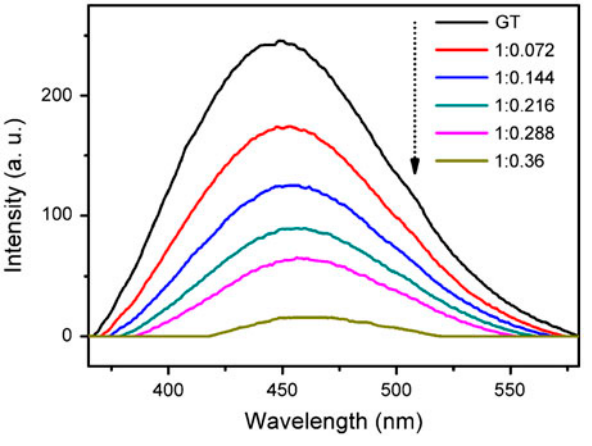

Figure 4. Fluorescence of GT was titrated by varying the concentration of SiW_{12} in aqueous solution. The molar ratios of GT and SiW_{12} range from 1 : 0.072, 1 : 0.144, 1 : 0.216, 1 : 0.288, to 1 : 0.36, respectively. As indicated by the dashed arrow, the fluorescence intensity of GT decreased gradually upon increasing the concentration of SiW_{12}.

carried out on *S. aureus* and *E. coli* using the plate disc method and the MIC. The inhibition zones after incubation of complexes are shown in figure 5. The results reveal that SiW_{12} and $CoCl_2$ have no bacterial activity against *E. coli* and *S. aureus* [figure 5(c) and (f)], but **1** and $Co(GT)_2$ exhibit similar activities to the free ligands (GT) against *S. aureus* and *E. coli* as shown in figure 5(a) and (b). The percentages of GT are 30 and 80% in **1** and $Co(GT)_2$, respectively. The antibacterial activity of **1** is similar to GT precursor. However, if the GT component in the complexes was controlled at the same molar concentration, as shown in figure 5(d) and (e), **1** generates the biggest antibacterial area during the Kirby–Bauer disc diffusion detection. This result indicates that the formation of ternary complex $[Co(GT)_3]$ as well as the introduction of polyoxoanion will synergistically enhance the antibacterial activity. The efficiencies of the complexes have been tested by applying MIC method ($\mu g\,mL^{-1}$) against *S. aureus* and *E. coli*. The MIC values against *E. coli* for **1**, $Co(GT)_2$, and GT are 2.42, 2.52, and 1.28 $\mu g\,mL^{-1}$, respectively. This result shows that **1**, $Co(GT)_2$, and GT all exhibit high antibacterial activities. However, the MIC values against *S. aureus* of **1** and $Co(GT)_2$ are 2.52 and 3.24 $\mu g\,mL^{-1}$, respectively, slightly different to 1.25 $\mu g\,mL^{-1}$ of GT.

It is instructive to compare our antibacterial activity to those of other floxacin complexes. Recently, many efforts have been devoted to the development of functional materials based on floxacin complexes. However, it should be noted that there are hundreds of papers about the synthesis of floxacin and antibacterial study over the past decades. Herein, we intended to focus on the comparison study on antibacterial activities of GT complexes, which belong to the third-generation quinolones. As summarized in table 1, entries 1, 3, 7, and 9 clearly

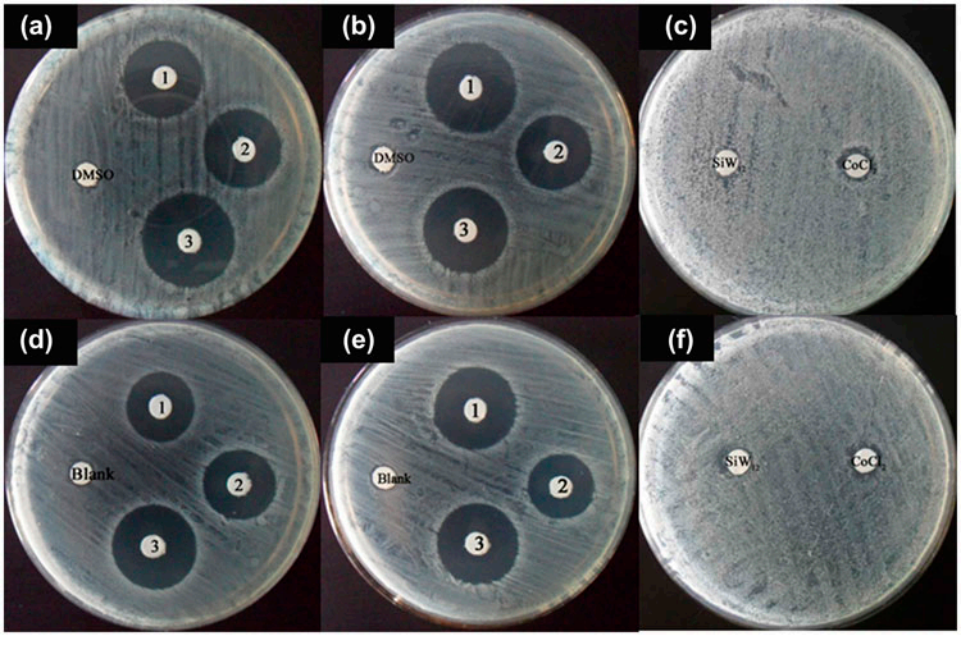

Figure 5. The inhibition zone of DMSO, 1 (complex **1**), 2 ($Co(GT)_2$), and 3 (GT) in [(a) and (d), at the same mass concentrations] and [(b) and (e), at the same molar concentrations of GT] and SiW_{12} and $CoCl_2$ in [(c) and (f)] against *E. coli* and *S. aureus*, respectively.

display that the MIC values of gatifoxacin varied because of the different test methodologies or experimental conditions, viz. it is difficult to compare these values for the antibacterial activities with those reported in other groups' work [7, 41, 42]. However, it is worth noting that the structural modification of GT enhanced the antibacterial activity in entries 2 and 8 (table 3). Meanwhile, as shown in entries 4 and 5 (table 3), the metal complexes of GT also gave better antibacterial activity than that of GT. Taking the experimental deviations into account, MIC values of **1** against *E. coli* and *S. aureus* in entry 11 (table 3) are comparable with the previous reported GT derivatives and metal complexes of GT based on the mass percentage of GT.

The introduction of the polyoxoanion into the metal complex may have a synergistic effect on its antibacterial activity. Apart from the effect of polyoxoanion, the different MIC values of **1** and $Co(GT)_2$ may be ascribed to the different coordination environments of their Co^{2+} cations. In $Co(GT)_2$, with cobalt ions and GT in a ratio of 1 : 2, Co^{2+} is four-coordinate by oxygens from carboxylate and water to form a planar structure. While in **1**, the ratio of cobalt ions and GT is 1 : 3 and the central Co^{2+} is six-coordinate by oxygens of GT ligands to form an octahedral geometry. Complex **1** exhibits higher antibacterial activity than that of $Co(GT)_2$, suggesting that different coordination modes of metal ions, combining with the introduction of POMs, may alter their biological activities.

3.6. *Interaction with DNA*

DNA can provide three distinct binding sites for quinolone metal complexes, groove binding, binding to phosphate and intercalation [43]. This behavior is of great importance with regard to the relevant biological role of quinolone antibiotics in the body. UV spectra of the interaction of CT-DNA with GT, **1**, and $Co(GT)_2$ have been recorded for a constant CT-DNA concentration in different [complex]/[DNA] mixing ratios as shown in figure 6(a)–(c). The changes can be observed in the absorption spectra of CT-DNA in the presence of GT, **1**, and $Co(GT)_2$. The decrease in the intensity at $\lambda_{max} = 258$ nm indicates interaction of GT, **1**, and $Co(GT)_2$ with CT DNA, resulting in the formation of a new complex with double-helical CT-DNA [44]. In figure 6(d)–(f), the changes occurred in the spectra of GT, **1**, and $Co(GT)_2$ during the titration upon addition of CT-DNA in diverse concentrations, respectively. In the UV region, the intense absorption bands observed in the spectrum at 286 and

Table 3. MIC values of GT, GT derivatives, metal–GT complexes, and **1**.

		MIC ($\mu g\,mL^{-1}$)		
Entry	Compounds	*E. coli*	*S. aureus*	Ref.
1	GT	2–4	0.125	[41]
2	GT derivatives	0.25–128	0.06–128	[41]
3	GT	–	0.3125	[7]
4	$Zn(GT)_2$	–	0.3125 (0.2541)[a]	[7]
5	$Ni(GT)_2$	–	0.3125 (0.2531)[a]	[7]
6	$Co(GT)_2$	–	0.625 (0.5063)[a]	[7]
7	GT	1	0.25	[42]
8	Thiadiazole–GT hybrids	1–64	0.125–64	[42]
9	GT	1.28	1.25	This work
10	$Co(GT)_2$	2.52 (2.016)[a]	3.24 (2.592)[a]	This work
11	**1**	2.42 (0.726)[a]	2.52 (0.756)[a]	This work

[a]MIC values are calculated based on mass percentage of GT.

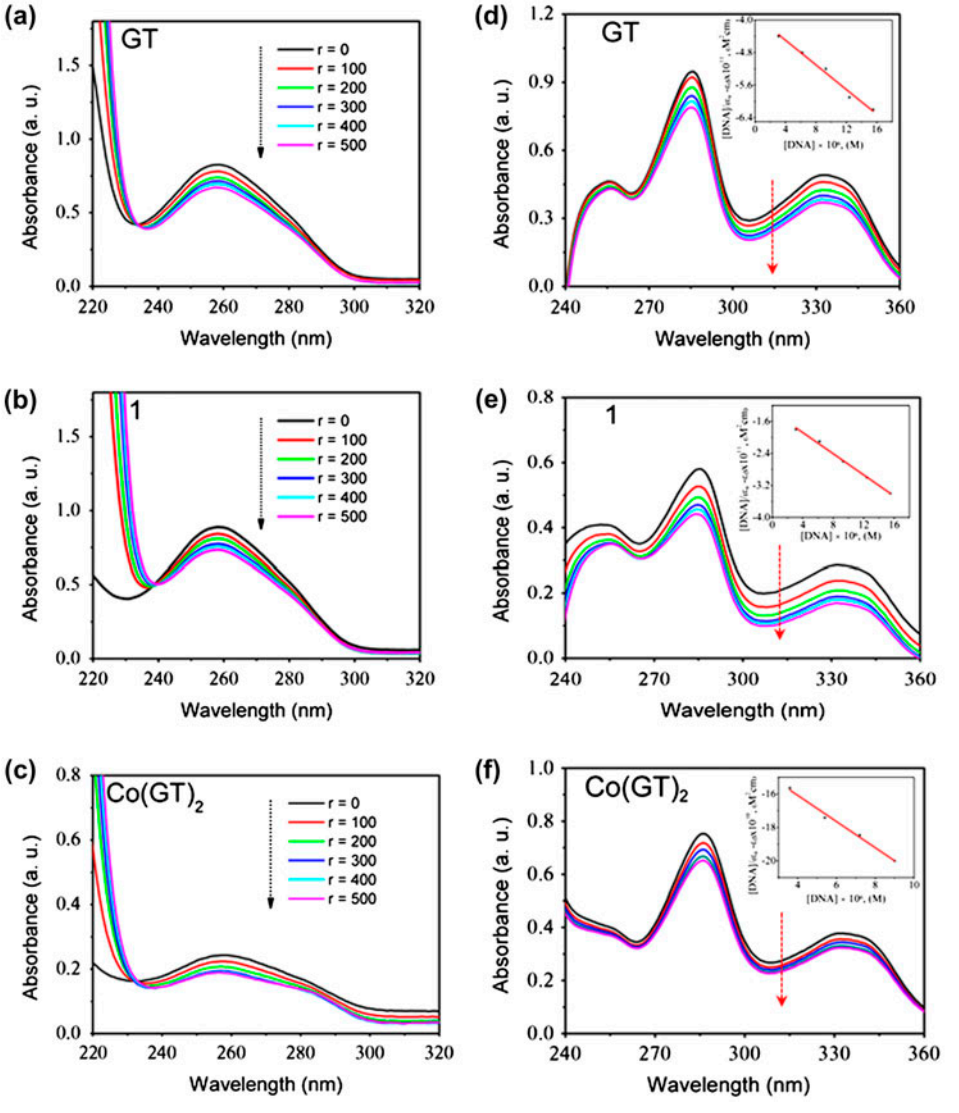

Figure 6. UV spectra of CT-DNA in buffer solution in the absence or presence of (a) GT ([DNA] = 1.25×10^{-4} M L^{-1}), (b) **1** ([DNA] = 1.35×10^{-4} M L^{-1}), and (c) Co(GT)$_2$ ([DNA] = 3.6×10^{-5} M L^{-1}). The black arrows show the changes upon increasing the amounts of the compounds; r represents the ratio of complex to CT-DNA. UV spectra of (d) GT (7.5×10^{-7} M L^{-1}), (e) **1** (3×10^{-6} M L^{-1}), and (f) Co(GT)$_2$ (3×10^{-5} M L^{-1}) in DMSO solution in the presence of CT-DNA at increasing amounts. The red arrows show the changes upon increasing the amounts of CT-DNA. Insets are the plots of $\frac{[DNA]}{(\varepsilon_a - \varepsilon_f)}$ *vs.* [DNA].

333 nm for GT, 285, and 332 nm for **1**, and 286 and 332 nm for Co(GT)$_2$ are attributed to the π–π^* transition of the coordinated groups of GT [45]. When the concentration of CT-DNA increased, hypochromism with a negligible red shift is observed at the maximum. The intensity of the band is decreased and a slight red shift is observed in the presence of

increasing amounts of CT-DNA. This result suggests intercalation of GT, **1**, and $Co(GT)_2$ with DNA involving a strong $\pi\cdots\pi$ stacking interaction between an aromatic chromophore and the base pairs of DNA [46]. The binding constant K_b can be obtained by the ratio of slope to the intercept of the y axis in plots of $\frac{[DNA]}{(\varepsilon_a-\varepsilon_f)}$ *versus* [DNA], according to the following equation [47]:

$$\frac{[DNA]}{(\varepsilon_a-\varepsilon_f)}=\frac{[DNA]}{(\varepsilon_b-\varepsilon_f)}+\frac{1}{K_b(\varepsilon_a-\varepsilon_f)}$$

where $\varepsilon_a = A_{obsd}/[(compounds)]$, ε_f = extinction coefficient for the free complex, and ε_b = extinction coefficient for the complex in the fully bound form.

The obtained K_b value, 9.6×10^4, of **1** is higher than those of GT (3.8×10^4) and Co $(GT)_2$ (6×10^4), which suggests its strong binding interaction to CT-DNA. This result indicates that the formation of tris complex $[Co(GT)_3]$ and the introduction of POMs can significantly enhance DNA binding.

4. Conclusion

POM-based **1** has been isolated for the first time, containing unusual $[Co(GT)_3]$ subunits. The possible energy transfer or electron transfer has been confirmed by changes of characteristic peaks in FT-IR and efficient fluorescence quenching. Additionally, interaction of **1** with CT-DNA has been studied by UV spectroscopy and indicates that **1** exhibits higher binding constant to CT-DNA than its parent GT. The antibacterial activity of **1** shows a slight decrease in its antibacterial potential as compared with GT. However, **1** can greatly save the cost, which opens a new way to design POM-induced low-cost antibacterial inorganic–organic hybrids.

Supplementary material

Crystallographic data have been deposited with the Cambridge Crystallographic Data Center. The CCDC number of **1** is 855046. Copy of the data can be obtained free of charge on application to The Director, CCDC, 12 Union Road, Cambridge CB2, 1EZ, UK (Fax: +44 1223 336033); E-mail: deposit@ccdc.cam.ac.uk or http://www.ccdc.cam.ac.uk).

Funding

We acknowledge the National Natural Science Foundation of China [grant number 21271034], [grant number 21103035], Heilongjiang Province Natural Science Funds for Distinguished Young Scholar [grant number JC201220], Natural Science Foundation of Heilongjiang Province [grant number QC2011C038], Heilongjiang Universities' Science and Technology Innovation Team program [grant number 2012TD010], and financial supports from the Fundamental Research Funds for the Central Universities [grant number HIT. NSRIF. 2011025], SKLUWRE of HIT (QA201022), China Postdoctoral Science Foundation [grant number 20100471060], [grant number 2012T50313].

References

[1] J.H.M. Cabral, A.P. Jackson, C.V. Smith, N. Shikotra, A. Maxwell, R.C. Liddington. *Nature*, **388**, 903 (1997).
[2] M. Čižman. *Int. J. Antimicrob. Agents*, **21**, 297 (2003).
[3] K. Yamaguchi, A. Ohno. *Diagn. Microbiol. Infect. Dis.*, **52**, 135 (2005).
[4] D.C. Hooper. *Lancet. Infect. Dis.*, **2**, 530 (2002).
[5] F. Gao, P. Yang, J. Xie, H. Wang. *J. Inorg. Biochem.*, **60**, 61 (1992).
[6] L.A. Mandell. *Diagn. Microbiol. Infect. Dis.*, **44**, 65 (2002).
[7] Z.-Q. Li, F.-J. Wu, Y. Gong, C.-W. Hu, Y.-H. Zhang, M.-Y. Gan. *Chin. J. Chem.*, **25**, 1809 (2007).
[8] M.N. Patel, D.S. Gandhi, P.A. Parmar. *Inorg. Chem. Commun.*, **15**, 248 (2012).
[9] E.K. Efthimiadou, Y. Sanakis, N. Katsaros, A. Karaliota, G. Psomas. *Polyhedron*, **26**, 1148 (2007).
[10] E.K. Efthimiadou, A. Karaliota, G. Psomas. *Polyhedron*, **27**, 1729 (2008).
[11] Z. An, W. Xu, R.-S. Wang. *Acta Crystallogr., Sect. E*, **63**, m507 (2007).
[12] J.T. Rhule, C.L. Hill, D.A. Judd, R.F. Schinazi. *Chem. Rev.*, **98**, 327 (1998).
[13] M.S. Weeks, C.L. Hill, R.F. Schinazi. *J. Med. Chem.*, **35**, 1216 (1992).
[14] V. Artero, A. Proust, P. Herson, F. Villain, C. Cartier dit Moulin, P. Gouzerh. *J. Am. Chem. Soc.*, **125**, 11156 (2003).
[15] X. Wang, J. Liu, M.T. Pope. *Dalton Trans.*, 957 (2003).
[16] S. Upreti, A. Ramanan. *Cryst. Growth Des.*, **5**, 1837 (2005).
[17] C.-Y. Sun, S.-X. Liu, D.-D. Liang, K.-Z. Shao, Y.-H. Ren, Z.-M. Su. *J. Am. Chem. Soc.*, **131**, 1883 (2009).
[18] F.-J. Ma, S.-X. Liu, C.-Y. Sun, D.-D. Liang, G.-J. Ren, F. Wei, Y.-G. Chen, Z.-M. Su. *J. Am. Chem. Soc.*, **133**, 4178 (2011).
[19] J.-Q. Sha, L.-Y. Liang, P.-F. Yan, G.-M. Li, C. Wang, D.-Y. Ma. *Polyhedron*, **31**, 422 (2012).
[20] J.-Q. Sha, L.-Y. Liang, X. Li, Y. Zhang, H. Yan, G. Chen. *Polyhedron*, **30**, 1657 (2011).
[21] J.-Q. Sha, X. Li, Y.-H. Zhou, P.-F. Yan, G.-M. Li, C. Wang. *Solid State Sci.*, **13**, 1972 (2011).
[22] A. Tézé, G. Hervé. *J. Inorg. Nucl. Chem.*, **39**, 999 (1977).
[23] J. Marmur. *J. Mol. Biol.*, **3**, 208 (1961).
[24] M.E. Reichmann, S.A. Rice, C.A. Thomas, P. Doty. *J. Am. Chem. Soc.*, **76**, 3047 (1954).
[25] G.M. Sheldrick. *SHELXS-97, Program for Crystal Structure Solution*, University of Göttingen, Göttingen (1997).
[26] G.M. Sheldrick. *SHELX-97, Program for Crystal Structure Refinement*, University of Göttingen, Göttingen (1997).
[27] N. Jiménez-Garrido, L. Perelló, R. Ortiz, G. Alzuet, M. González-Álvarez, E. Cantón, M. Liu-González, S. García-Granda, M. Pérez-Priede. *J. Inorg. Biochem.*, **99**, 677 (2005).
[28] C. Chulvi, M.C. Muñoz, L. Perelló, R. Ortiz, M.C. Muñoz, M.I. Arriortua, J. Via, K. Urtiaga, J.M. Amigó, L.E. Ochando. *J. Inorg. Biochem.*, **42**, 133 (1991).
[29] I.D. Brown, D. Altermatt. *Acta Crystallogr., Sect. B*, **41**, 244 (1985).
[30] X.-l. Wang, J. Li, A.-x. Tian, D. Zhao, G.-c. Liu, H.-y. Lin. *Cryst. Growth Des.*, **11**, 3456 (2011).
[31] Y. Yang, L. Xu, F. Li, X. Du, Z. Sun. *J. Mater. Chem.*, **20**, 10835 (2010).
[32] X. Xing, R. Liu, X. Yu, G. Zhang, H. Cao, J. Yao, B. Ren, Z. Jiang, H. Zhao. *J. Mater. Chem. A*, **1**, 1488 (2012).
[33] B. Qin, H. Chen, H. Liang, L. Fu, X. Liu, X. Qiu, S. Liu, R. Song, Z. Tang. *J. Am. Chem. Soc.*, **132**, 2886 (2010).
[34] R. Liu, X. Yu, G. Zhang, S. Zhang, H. Cao, A. Dolbecq, P. Mialane, B. Keita, L. Zhi. *J. Mater. Chem. A*, **1**, 11961 (2013).
[35] Y. Qiu, L. Xu, G. Gao, W. Wang, F. Li. *Inorg. Chim. Acta*, **359**, 451 (2006).
[36] H. Gu, L. Bi, Y. Fu, N. Wang, S. Liu, Z. Tang. *Chem. Sci.*, **4**, 4371 (2013).
[37] F. Dimiza, F. Perdih, V. Tangoulis, I. Turel, D.P. Kessissoglou, G. Psomas. *J. Inorg. Biochem.*, **105**, 476 (2011).
[38] F. Dimiza, A.N. Papadopoulos, V. Tangoulis, V. Psycharis, C.P. Raptopoulou, D.P. Kessissoglou, G. Psomas. *Dalton Trans.*, 4517 (2010).
[39] I. Turel, A. Golobič, A. Klavžar, B. Pihlar, P. Buglyó, E. Tolis, D. Rehder, K. Sepčić. *J. Inorg. Biochem.*, **95**, 199 (2003).
[40] M.P. López-Gresa, R. Ortiz, L. Perelló, J. Latorre, M. Liu-González, S. García-Granda, M. Pérez-Priede, E. Cantón. *J. Inorg. Biochem.*, **92**, 65 (2002).
[41] Y. Chai, M.-L. Liu, K. Lv, L.-S. Feng, S.-J. Li, L.-Y. Sun, S. Wang, H.-Y. Guo. *Eur. J. Med. Chem.*, **46**, 4267 (2011).
[42] S. Jazayeri, M.H. Moshafi, L. Firoozpour, S. Emami, S. Rajabalian, M. Haddad, F. Pahlavanzadeh, M. Esnaashari, A. Shafiee, A. Foroumadi. *Eur. J. Med. Chem.*, **44**, 1205 (2009).
[43] B.M. Zeglis, V.C. Pierre, J.K. Barton. *Chem. Commun.*, **44**, 4565 (2007).
[44] G.S. Son, J.-A. Yeo, M.-S. Kim, S.K. Kim, A. Holmén, B. Åkerman, B. Nordén. *J. Am. Chem. Soc.*, **120**, 6451 (1998).

[45] E.K. Efthimiadou, Y. Sanakis, M. Katsarou, C.P. Raptopoulou, A. Karaliota, N. Katsaros, G. Psomas. *J. Inorg. Biochem.*, **100**, 1378 (2006).
[46] M. Baldini, M. Belicchi-Ferrari, F. Bisceglie, P.P. Dall'Aglio, G. Pelosi, S. Pinelli, P. Tarasconi. *Inorg. Chem.*, **43**, 7170 (2004).
[47] A.M. Pyle, J.P. Rehmann, R. Meshoyrer, C.V. Kumar, N.J. Turro, J.K. Barton. *J. Am. Chem. Soc.*, **111**, 3051 (1989).